D3140 | EGU2020-55, https://doi.org/10.5194/egusphere-egu2020-55
EGU General Assembly, Wien, Austria, 4 – 8 May 2020
AS1.34 Joint Session of the MLT and the VarSITI-ROSMIC program

Seasonal-latitudinal distributions of the populations of the states $O_2(b^1\Sigma^+_g, v' = 0 – 2)$ in the daytime mesosphere and lower thermosphere

Rada Manuilova and Valentine Yankovsky

St-Petersburg State University, St. Petersburg, Russian Federation
(nansey@yandex.ru)

In the last decade, it was shown that volume emission rates (VMR) for transitions from the levels $O_2(b^1\Sigma_g^+, v = 0 – 2)$ to the levels $O_2(X^3\Sigma_g^-, v=0)$ can be used as proxies for retrieving the altitude profiles of $[O(^3P)]$, $[O_3]$ and $[CO_2]$ in the mesosphere and lower thermosphere (MLT) [Yankovsky et al., 2016; Yankovsky and Manuilova, 2018, Yankovsky et al., 2019]. Despite the fact that, in single experiments, radiation in the bands 762, 688, and 628 nm corresponding to the abovementioned transitions was observed, no systematic measurements of the intensities of these emissions have yet been performed. The main source of excitation of the levels $O_2(b^1\Sigma_g^+, v = 0 – 2)$ is the energy transfer from the excited $O(^1D)$ atom, along with the resonant absorption of solar radiation in these bands in the mesosphere. Within the framework of the YM2011 model of electronical-vibrational kinetics of the excited products of O_2 and O_3 photolysis, we calculated the altitudinal-latitudinal distributions of the $[O(^1D)]$, $[O_2(b^1\Sigma_g^+, v = 0)]$, $[O_2(b^1\Sigma_g^+, v = 1)]$ and $[O_2(b^1\Sigma_g^+, v = 2)]$ using, as an example, the atmospheric conditions of the TIMED/SABER satellite experiment for the SABER 2010 events.

1. Model of electronic-vibrational kinetics of the products of O_3 and O_2 photolysis in the MLT YM2011

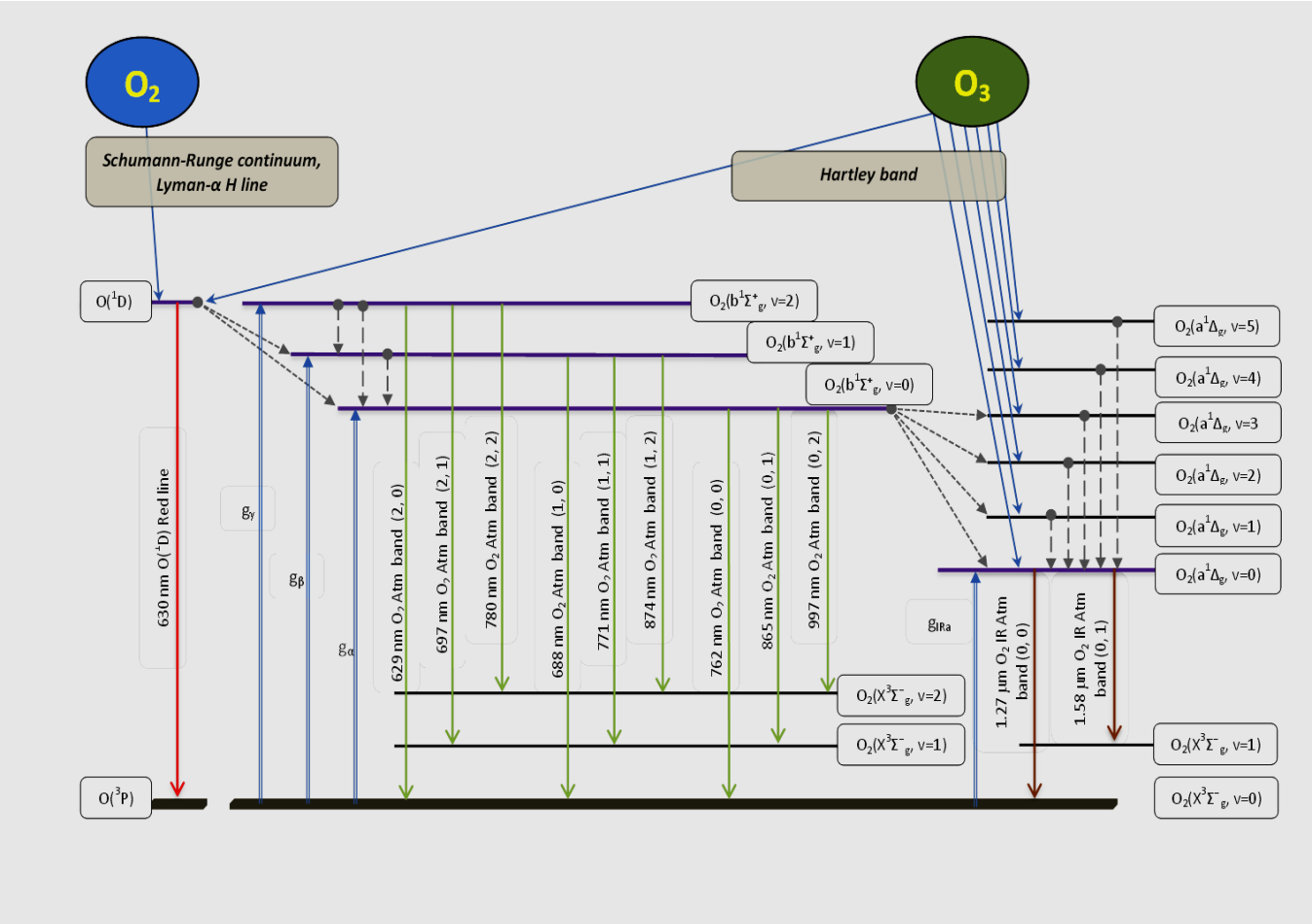

Fig.1. Scheme of kinetics of 10 excited levels of YM2011 model: $O(^1D)$, three levels $O_2(b^1\Sigma^+_g, v=0-2)$ and six levels $O_2(a^1\Delta_g, v=0-5)$.
Blue lines – the processes of O_2 and O_3 photolysis. Double blue lines with upward arrows – the processes of solar radiation absorption in the 762 nm (g_α), 688 nm (g_β), 629 nm (g_γ) and in the 1.27 μm (g_{IRa}) bands. Dotted lines with arrows – collisional energy transitions from $O(^1D)$ to the $O_2(b^1\Sigma^+_g, v=0, 1)$ and from $O_2(b^1\Sigma^+_g, v=0)$ to $O_2(a^1\Delta_g, v=0-3)$. Dashed vertical lines with arrows – collisional V-V transitions. Solid red vertical lines – the processes of radiative emissions from electronic-vibrational levels of O_2 and from excited atom $O(^1D)$.

Fig. 1 shows the scheme of energy transfer between the products of O_3 and O_2 photolysis leading to the formation of electronically-vibrationally excited molecules in the $O_2(b^1\Sigma^+_g, v \le 2)$ and $O_2(a^1\Delta_g, v \le 5)$ states, as well as the $O(^1D)$ atom. The traditional channel of the $O_2(a^1\Delta_g, v)$ excitation is O_3 photolysis in the singlet channel. The alternative channel of the $O_2(a^1\Delta_g, v = 0)$ excitation is multistage. As can be seen from the scheme, the levels $O_2(b^1\Sigma^+_g, v = 0, 1)$ are

excited due to the energy transfer from the $O(^1D)$ atom formed during the photolysis of O_2 and O_3. Further, the energy of the level $O_2(b^1\Sigma^+_g, v = 0)$ goes to the excitation of the levels $O_2(a^1\Delta_g, v = 0 – 3)$ with subsequent collisional relaxation to the level $O_2(a^1\Delta_g, v = 0)$. The processes of exciting and quenching of all these levels are described by more than seventy photochemical reactions. In [Yankovsky et al., 2016; Yankovsky and Manuilova, 2018] within the framework of the YM2011 model, we presented the databases on the values of the rate coefficients and quantum yields of the reaction products with their errors. In [Yankovsky et al., 2016] we presented the complete kinetic equations for populations of ten excited levels ($O(^1D)$, $O_2(b^1\Sigma^+_g, v = 0 – 2)$, $O_2(a^1\Delta_g, v = 0 – 5)$). In the present study we used these equations to solve the forward problem. The rate coefficients for reactions involving $O(^1D)$, $O_2(b^1\Sigma^+_g, v = 0 – 2)$, $O_2(a^1\Delta_g, v = 0, 1)$ in the processes of radiative quenching and deexcitation at collisions with $O(^3P)$, O_2, O_3, N_2, CO_2 are presented in the Table 1 [Yankovsky and Manuilova, 2018].

Figures 2–6 show the calculations of the altitude profiles of $O(^1D)$, $O_2(b^1\Sigma^+_g, v = 0)$, $O_2(b^1\Sigma^+_g, v =1)$ and $O_2(b^1\Sigma^+_g, v = 2)$ concentrations performed for the atmospheric conditions of the TIMED/SABER experiment for the days of Vernal equinox, Autumn equinox, Summer solstice, and Winter solstice. Figure 2 shows the values averaged over all daylight hours for all SABER events for these days. Figures 3–6 show the values for the day of Vernal equinox averaged over the calculated values for SABER events grouped by close latitudes.

2. Seasonal-latitudinal distributions of the populations of the levels $O(^1D)$, $O_2(b^1\Sigma^+_g, v' = 0 – 2)$ in the daytime MLT

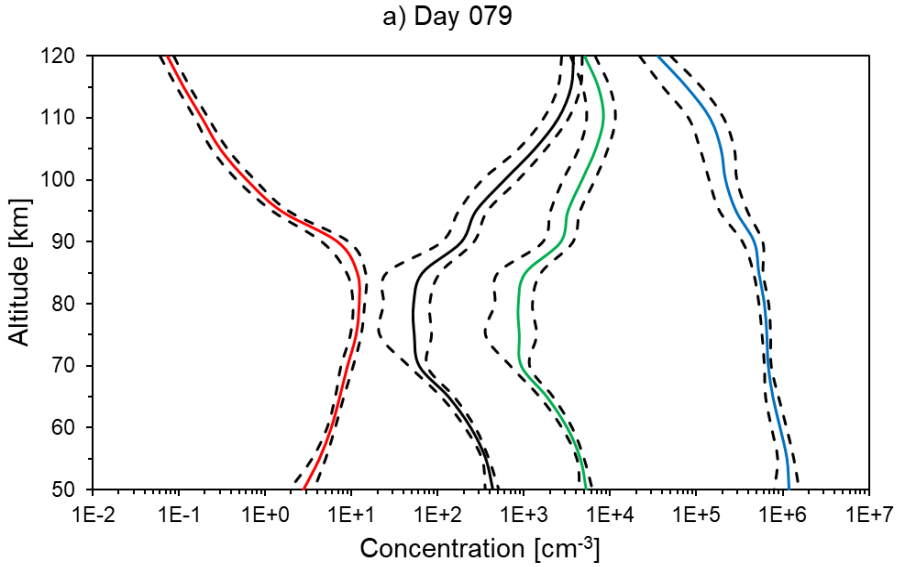

Fig. 2a. Daily mean altitude profiles of $O_2(b^1\Sigma_g^+, v = 0)$, $O_2(b^1\Sigma_g^+, v = 1)$, $O_2(b^1\Sigma_g^+, v = 2)$, $O(^1D)$ concentrations and their standard deviations (dashed lines) calculated via YM2011 based on TIMED-SABER data for 4 days in 2010. Black solid line – $[O(^1D)]$, blue line – $[O_2(b^1\Sigma_g^+, v = 0)]$, green line – $[O_2(b^1\Sigma_g^+, v = 1)]$, red line $[O_2(b^1\Sigma_g^+, v = 2)]$. Vernal equinox (Day 079).

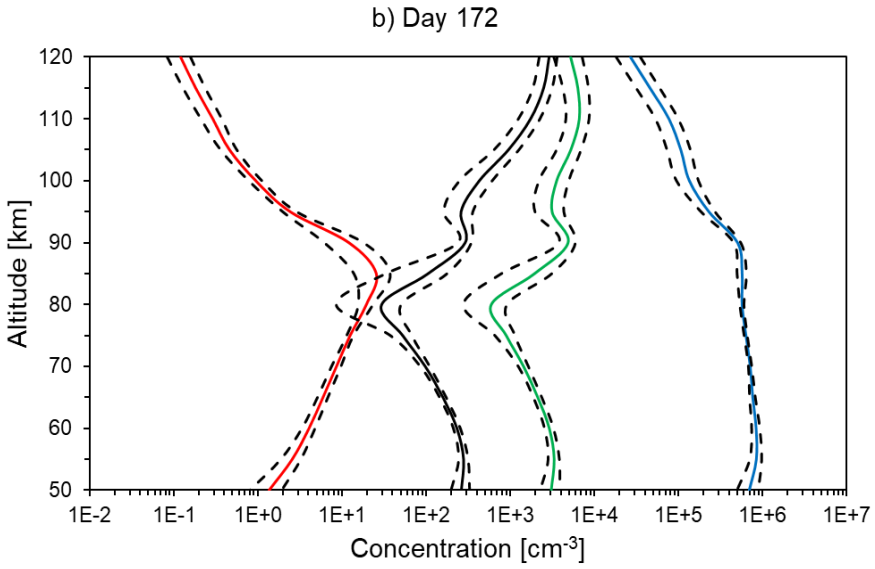

Fig. 2b. The same as in Fig. 2a, for Summer solstice (Day 172).

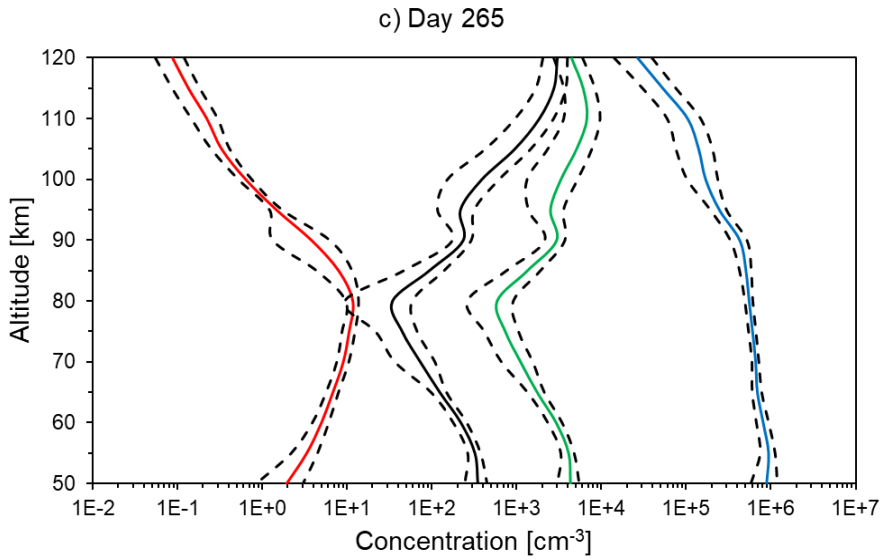

Fig. 2c. The same as in Fig. 2a, for Autumn equinox (Day 265).

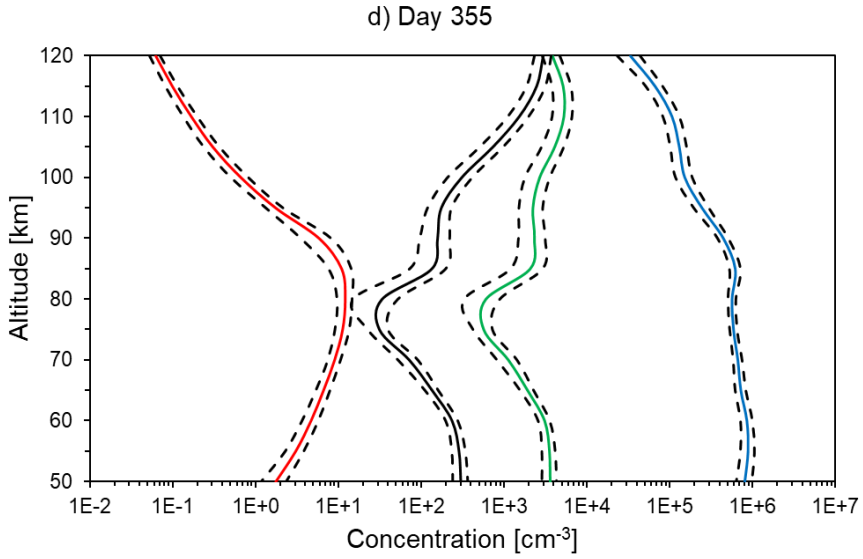

Fig. 2d. The same as in Fig. 2a, for Winter solstice (Day 365).

The altitude profile of the $O_2(b^1\Sigma_g^+, v = 0)$ concentration is practically independent of the season and weakly correlates with the altitude profile of the $O(^1D)$ concentration; on the contrary, the $[O_2(b^1\Sigma_g^+, v = 1)]$ altitude profile strongly correlates with the $[O(^1D)]$ profile, since the main source of population of the $O_2(b^1\Sigma_g^+, v = 1)$ is the energy transfer channel from $O(^1D)$ to $O_2(b^1\Sigma_g^+, v = 1)$. A change in the altitude of the $O_2(b^1\Sigma_g^+, v = 2)$ concentration maximum in the range of 70-90 km for different seasons is most likely associated with a change in the solar radiation spectrum, since the absorption of solar radiation in the band at wavelength of 629 nm plays the main role in the excitation of the $O_2(b^1\Sigma_g^+, v = 2)$.

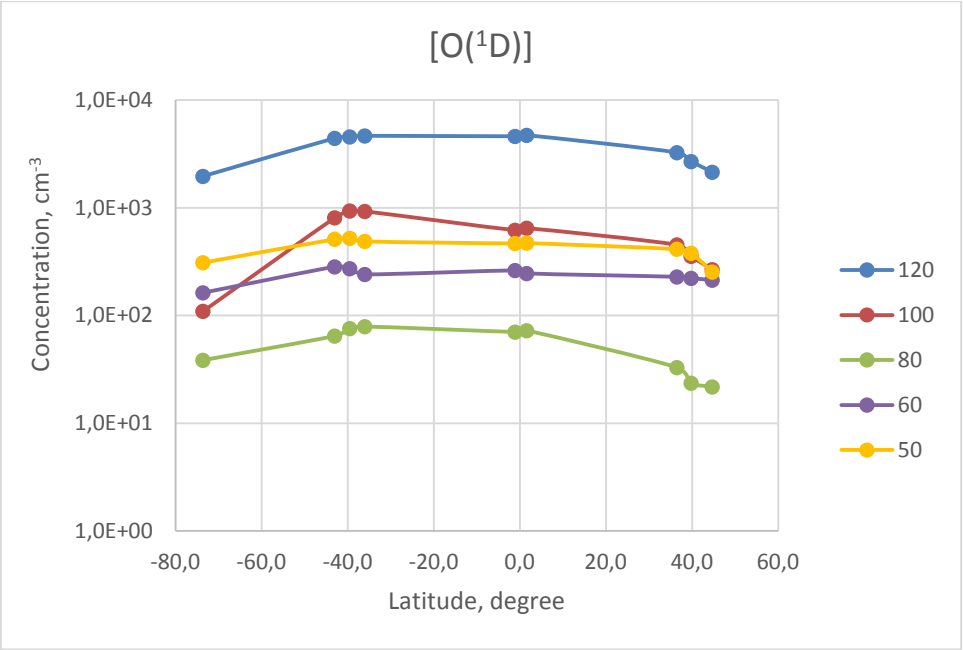

Fig. 3. Latitudinal dependence of [O(^{1}D)] for altitudes: 50, 60, 80, 100 and 120 km.

The main processes of O(^{1}D) formation are as follows: above 80 km, oxygen photolysis in the Schumann - Runge bands, below 80 km, the ozone concentration increases and the main process of O(^{1}D) formation becomes ozone photolysis in the Hartley bands. In the altitude range of 50 - 100 km O(^{1}D) deactivation occurs by 80% in collisions with N_2 molecules and 20% in collisions with O_2 molecules. Above 100 km the deactivation process in collisions with O(^{3}P) atoms is added, and at 120 km O(^{1}D) deactivation occurs by 70% in collisions with N_2, about 20% in collisions with O_2 and 10% in collisions with O(^{3}P).

Correspondingly, according to calculations in the framework of the YM2011 model, in the altitude range of 50-120 km, the highest concentration of O(^{1}D) is observed at an altitude of 120 km. With an increase of the deactivation rate by 100 km [O(^{1}D)] becomes about an order of magnitude lower for all latitudes, and at an altitude of 80 km, the minimum concentration is observed, which is explained by both an increase in the deactivation rate with increasing density and a low ozone concentration. Below 70 km, the O_3 concentration increases sharply and O_3 photolysis becomes the main source of O(^{1}D), therefore, at 60 km we see a sharp increase in the O(^{1}D) concentration, and at 50 km the [O(^{1}D)] values become close to 100 km.

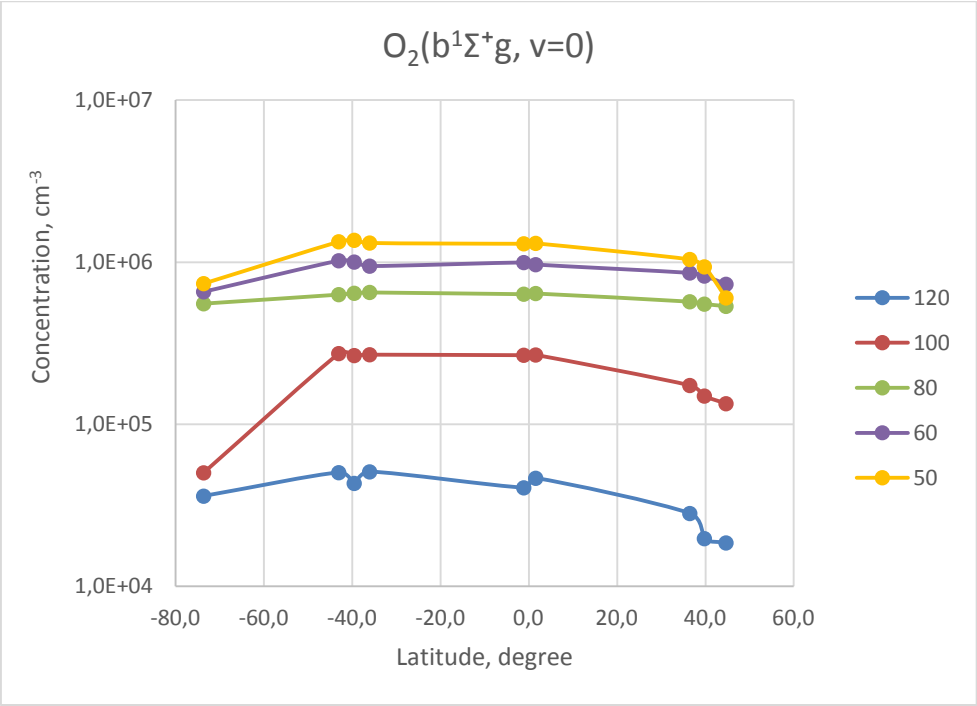

Fig. 4. Latitudinal dependence of [$O_2(b^1\Sigma_g^+, v=0)$] for altitudes: 50, 60, 80, 100 and 120 km.

Figures 4 and 5 show the latitudinal dependences of the concentrations of $O_2(b^1\Sigma_g^+, v = 0)$ and $O_2(b^1\Sigma_g^+, v = 1)$ for various altitudes. Above 85 km, the main process of population of $O_2(b^1\Sigma_g^+, v = 0, 1)$ is the reaction $O(^1D) + O_2(X^3\Sigma_g^-, v=0) \rightarrow O_2(b^1\Sigma_g^+, v = 0,1) + O(^3P)$. Below 100 km, the contribution of the processes of $O_2(b^1\Sigma_g^+, v = 0,1)$ population due to the absorption of solar radiation at 762 nm and 689 nm becomes important. Below 80 km, the $O(^1D)$ formation channel in the O_2 photolysis in the Schumann-Runge continuum, which dominates at high altitudes, gives way to $O(^1D)$ formation during the ozone photolysis in the Hartley band. The main contribution to the quenching of $O_2(b^1\Sigma_g^+, v = 0)$ at 120 km is associated with the radiation process, to which quenching in collisions with $O(^3P)$ atoms and N_2 molecules is added at 100 km.

Correspondingly, at 120 km [$O_2(b^1\Sigma_g^+, v = 0)$] falls by almost an order of magnitude compared with a concentration of 100 km at the corresponding latitudes. Below 80 km, on the one hand, the quenching rate of the $O_2(b^1\Sigma_g^+, v = 0)$ in collisions with nitrogen molecules sharply increases; on the other hand, the $O_2(b^1\Sigma_g^+, v = 0)$ excitation rate increases below 70 km due to an increase of ozone concentration, since this leads to an increase in the rate of $O(^1D)$ formation at photolysis of ozone in the Hartley band. The combination of these processes leads

to the fact that the difference in the values of [$O_2(b^1\Sigma_g^+$, v = 0)] at altitudes of 80, 60, and 50 km is relatively small for the corresponding latitudes.

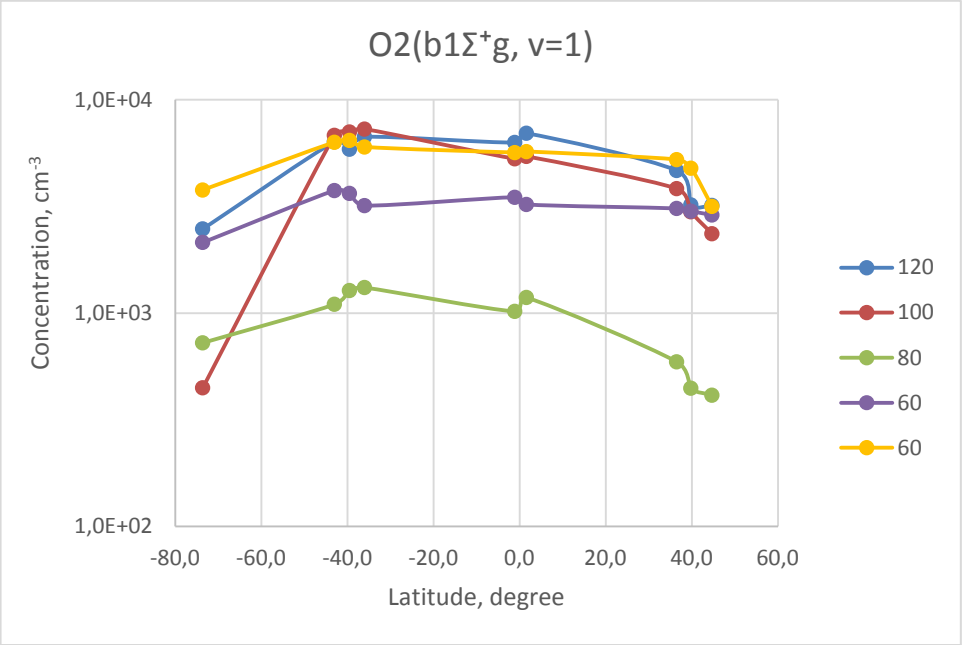

Fig. 5. Latitudinal dependence of [$O_2(b^1\Sigma_g^+$, v=1)] for altitudes: 50, 60, 80, 100 and 120 km.

Despite the fact that the excitation processes of $O_2(b^1\Sigma_g^+$, v = 1) and $O_2(b^1\Sigma_g^+$, v = 0) are the same, the behavior of the curves of the latitudinal dependence of concentrations for different altitudes varies significantly. Below 90 km, as the O_2 concentration increases, the rate at which the $O_2(b^1\Sigma_g^+$, v = 1) concentration decreases sharply increases, compared to the rate of decrease in $O_2(b^1\Sigma_g^+$, v = 0) concentration. This is determined by the quick reaction of EE exchange $O_2(b^1\Sigma_g^+$, v = 1)] + $O_2(X^3S^-_g$, v=0) → $O_2(X^3\Sigma_g^-$, v=1) + $O_2(b^1\Sigma_g^+$, v = 0). In this regard, [$O_2(b^1\Sigma_g^+$, v = 1)] is minimal at 80 km in the range 50 - 120 km at almost all latitudes. Below 70 km, as mentioned above, [$O_2(b^1\Sigma_g^+$, v = 1)] increases due to a sharp increase in ozone concentration (curves for 60 and 50 km). It is interesting that the values of [$O_2(b^1\Sigma_g^+$, v = 1)] for altitudes of 120, 100 and 50 km (for mid-latitudes) are close to each other. The fact is that the main process of population of $O_2(b^1\Sigma_g^+$, v=0, 1) above 85 km is the reaction $O(^1D) + O_2(X^3\Sigma_g^-$, v=0) → $O_2(b^1\Sigma_g^+$, v = 0,1) + $O(^3P)$, in which the quantum yield of $O_2(b^1\Sigma_g^+$, v = 1) is 0.8, so the relative contribution of this process to the population of $O_2(b^1\Sigma_g^+$, v = 1)] is much more than in the population of $O_2(b^1\Sigma_g^+$, v = 0) which leads to the values of [$O_2(b^1\Sigma_g^+$, v = 1)] at 120 km, which are close to the values at 100 and 50 km.

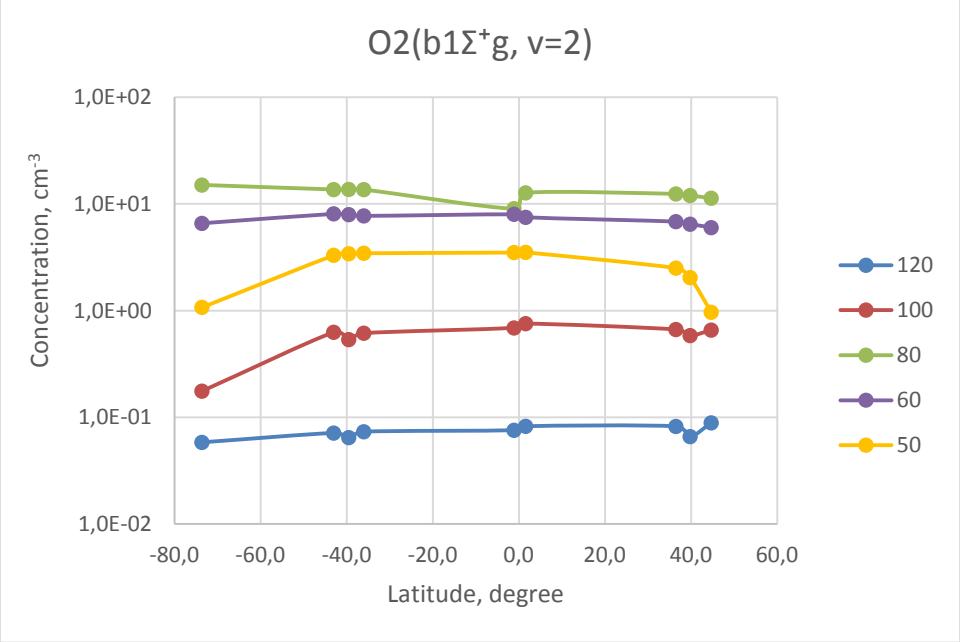

Fig. 6. Latitudinal dependence of [$O_2(b^1\Sigma_g^+$, v=2)] for altitudes: 50, 60, 80, 100 and 120 km.

In the excitation of the $O_2(b^1\Sigma_g^+$, v = 2) the main role is played by the absorption of solar radiation in the band at a wavelength of 629 nm, therefore, the low values of [$O_2(b^1\Sigma_g^+$, v = 2)] at altitudes of 120 and 100 km are explained by a decrease in the oxygen concentration above 90 km. Below 85 km, deactivation of $O_2(b^1\Sigma_g^+$, v = 2) occurs in collisions with O_2 molecules; above 90 km, a fast deactivation process in a collisions with $O(^3P)$ atoms is added, so the small maximum of [$O_2(b^1\Sigma_g^+$, v = 2)] values appears in the region of 60 - 90 km, which can be seen in Fig. 6, where the maximum values of [$O_2(b^1\Sigma_g^+$, v = 2)] correspond to an altitude of 80 km.

The concentrations of all considered excited components, $O(^1D)$, $O_2(b^1\Sigma_g^+$, v = 0), $O_2(b^1\Sigma_g^+$, v = 1), and $O_2(b^1\Sigma_g^+$, v = 2), are characterized by a significant decrease at high latitudes of the southern hemisphere at all considered altitudes. Note, that on the day of Vernal equinox in the TIMED / SABER experiment there were few measurements at high latitudes of the northern hemisphere. The concentrations of $O(^1D)$, $O_2(b^1\Sigma_g^+$, v = 0), $O_2(b^1\Sigma_g^+$, v = 1) and $O_2(b^1\Sigma_g^+$, v = 2) vary slightly depending on latitude in the range - 40°─ 40° for the considered altitudes of 50 ─120 km.

Summary

The high concentration of $O_2(b^1\Sigma_g^+, v = 1)$ obtained in the calculations at middle and equatorial latitudes confirms the conclusion of ([Yankovsky et al., 2016; Yankovsky and Manuilova, 2018, Yankovsky et al., 2019]) that this excited component is the optimal proxy for retrieving the ozone concentration, and $O_2(b^1\Sigma_g^+, v = 2)$ is the optimal proxy for retrieving the concentration of atomic oxygen, $O(^3P)$, even for high latitudes.

References

1. Yankovsky, V.; Vorobeva, E.; Manuilova, R. New techniques for retrieving the [$O(^3P)$], [O_3] and [CO_2] altitude profiles from dayglow oxygen emissions: Uncertainty analysis by the Monte Carlo method. Advances in Space Research 2019, 64, 1948–1967. https://doi.org/10.1016/j.asr.2019.07.020.

2. Yankovsky, V. A.; Manuilova, R. O. Possibility of simultaneous [O_3] and [CO_2] altitude distribution retrievals from the daytime emissions of electronically-vibrationally excited molecular oxygen in the mesosphere. J. Atmosp. Sol. -Terrest. Phys. 2018, 179, 22–33. doi:10.1016/j.jastp.2018.06.008.

3. Yankovsky, V. A.; Martyshenko, K. V.; Manuilova, R. O.; Feofilov, A. G. Oxygen dayglow emissions as proxies for atomic oxygen and ozone in the mesosphere and lower thermosphere. J. Molec. Spectrosc. 2016, 327, 209–232. doi:10.1016/j.jms.2016.03.006.

This study was supported by the Russian Foundation for Basic Research (grant RFBR No. 20-05-00450 A).